

# Scientific Research Associates, inc.

50 Nye Road, P.O. Box 1058  
Glastonbury, CT 06033  
(203) 659-0333 FAX (203) 633-0676

NAS3-27378

FLOW IN SERPENTINE COOLANT PASSAGES WITH TRIP STRIPS

R94-9089-7

Technical Progress Narrative Report

Reporting Period November 1, 1994 to November 30, 1994

D.G-N. Tse

December 1994

Prepared for

NASA Lewis Research Center  
Cleveland, OH 44135

N95-70605

Unclas

29/34 0033908

(NASA-CR-197495) FLOW IN  
SERPENTINE COOLANT PASSAGES WITH  
TRIP STRIPS Technical Progress  
Report, 1 - 30 Nov. 1994 (Science  
Research Associates) 25 p

INTERIM  
TN 34-CR  
OCIT  
33908  
p. 25

# Scientific Research Associates, inc.

---

50 Nye Road, P.O. Box 1058  
Glastonbury, CT 06033  
(203) 659-0333 FAX (203) 633-0676

December 13, 1994

Dr. Phil Poinsatte  
NASA/Lewis Research Center  
Mail Stop 5-11  
21000 Brookpark Road  
Cleveland, OH 44135

Subject: Contract No. NAS3-27378; Technical Progress Report for period November 1, 1994 - November 30, 1994.

Dear Dr. Poinsatte:

Under the subject contract, an effort is being conducted at Scientific Research Associates, Inc. (SRA) to obtain flow field measurements in the coolant passage of a rotating turbine blade with ribbed walls, both in the stationary and rotating frames. The data obtained will be used for validation of computational tools and assessment of turbine blade cooling strategies.

During the current reporting period, Task 3 (Stationary measurements) was essentially completed and Task 4 (Rotating frame measurements) and Task 5 (Reports) were active. Selected velocity components at selected measurement planes, which provide insight to the flow, will be presented in this report; a more comprehensive set will be presented in the final report.

The configuration of the turbine blade passage model is given in Figures 1 and 2, and the measuring plane locations are given in Table 1. It should be noted that there are twelve distinct planes for the narrow channel inflow configuration, Fig. 1, and twelve distinct planes for the wide channel inflow configuration, Fig. 2. For each configuration, three of these planes would be repeated with an inlet screen in place, as per Table 1. The model has a W-shaped internal serpentine passage. The four-pass channel with three 180° turns is identical to that of Wagner, et al (1994) and was chosen to allow analyses of the velocity measurements corresponding to the heat transfer results obtained by Wagner, et al (1994). The first two legs of the passage have a rectangular cross-section of 1.0" x 0.5". The last two legs of the passage have a square cross-section of 0.5" x 0.5". Trips with a streamwise pitch to trip height ( $P/e = 5$ ) and trip height to coolant passage width ( $e/Z = 0.1$ ), were machined along the leading and trailing walls. These dimensions are typical of those used in turbine blade coolant passages. The trips on these

walls are staggered by the half-pitch. The trips are skewed at  $\pm 45^\circ$  to the cross-flow as shown in the figure and this allows the effect of trip orientation to be examined. Experiments were conducted with flow entering the model through the 0.5" x 0.5" square passage (Configuration A) and the 1.0" x 0.5" rectangular passage (Configuration B).

Velocity measurements were obtained with a Reynolds number ( $Re$ ) of 25,000, based on the hydraulic diameter of the half inch square passage. Figure 3 shows the coordinate system used in presenting the results. The first, second and third legs of the four pass passage will be referred to as the first, second and third passages respectively in later discussion. Streamwise distance ( $x$ ) from the entrance is normalized by the hydraulic diameter ( $D$ ). Vertical ( $y$ ) and tangential ( $z$ ) distances are normalized by the half passage height ( $H$ ) and width ( $Z$ ), respectively. For the  $x$  coordinate, streamwise is positive. For the  $U$  component, radially outward is positive. The  $y$  coordinate and  $V$  component are positive against gravity. The  $z$  coordinate and  $W$  component are positive in the direction of rotation. The velocities are normalized by the bulk mean velocity ( $U_b$ ) of  $3.44 \text{ ms}^{-1}$ , based on the half inch square passage. The contours of the 1.0" x 0.5" and 0.5" x 0.5" passages were evaluated from 9 x 11 and 11 x 11 measurement grids, respectively.

Figures 4 to 8 show the velocity contours obtained with configuration A. Figure 4 shows the mean and rms velocity contours obtained at location A1, 1  $D$  downstream of the inlet. The streamwise velocity contours show an almost uniform velocity distribution at the inlet. The vertical variation is less 10% and the  $1.1 U_b$  velocity peak is close to the lower wall. The vertical velocities in the lower half of the passage are close to zero. The maximum positive and negative velocities are found to be  $0.18 U_b$  and  $-0.15 U_b$ . They occur in the upper half of the passage where the streamwise velocities are 10% below the bulk mean. The streamwise and vertical velocity characteristics are consistent with the flow pattern exiting an S-bend, such as the bend upstream of the inlet between the model and the plenum. This is not shown in Figs. 1 and 2.

Figure 5 shows the mean and rms velocity contours obtained at location A2, 7  $D$  downstream inlet. Comparison of the streamwise velocity contours at 1 and 7 diameters downstream of the inlet shows that the high velocity region (achieving  $1.65 U_b$ ) has shifted to the upper wall. The streamwise flow development is large ( $>0.65 U_b$  within 6  $D$ ) and this is attributed to strong vertical convection. The vertical velocity contour shows downward velocity reaching  $0.95 U_b$  near the two walls and upward velocity of around  $0.6 U_b$  in the center of the passage, indicating the presence of a double vortex. Since this is upstream of the first passage bend, its presence is clearly due to the presence of the trips.

Figure 6 shows the mean and rms velocity contours obtained at location A3, 1 D upstream of the first turn. The streamwise velocity contours show two high velocity regions (both reaching  $1.50 U_b$ ) close to the leading and trailing walls. Large streamwise flow development is also present in the last 6 D of the first passage. Comparison of the vertical velocity contours of Figures 5 and 6 indicates the strength of the double vortex in the middle of the passage is roughly equal to that at the end. The trips led to the development of an asymptotic flow.

Figure 7 shows the mean and rms velocity contours obtained at location A5, 1 D downstream of the first turn. The streamwise velocity contours at this location (and those of Figure 8) are negative because the second passage is a radially inward flow passage. The high velocity region ( $-1.55 U_b$ ) is close to the upper wall. The convection of the high velocity region to the upper wall at the exit of the turn is attributed to the secondary flow generated by the C-turn. The vertical velocity contours show that the double vortex is considerably weakened as the flow progresses through the turn. The maximum upward velocity at the center of the passage has reduced from  $0.60 U_b$  to  $0.25 U_b$ . The maximum downward velocity near the walls has reduced from  $-0.85 U_b$  to  $-0.70 U_b$ . The secondary flow generated by the turn opposes the vortex generated in the first passage.

Figure 8 shows the mean and rms velocity contours obtained at location A6, 1 D upstream of the second turn. The streamwise velocity contours show high velocity regions ( $-1.55 U_b$ ) close to the leading and trailing walls towards the end of the second passage. The velocity characteristics are similar to those at the end of the first passage, Figure 6, indicating that the flow towards the end of the first and second passages is fully developed. The convection of the high velocity region from the upper wall at the beginning of the passage to the two side walls towards the end is attributed to the double vortex structure. Comparison of the vertical velocity contours of Figures 6 and 8 shows that the double vortex in both the first and second passages circulate in the same direction with similar vortex strength.

Figures 9 to 14 show the velocity contours obtained with Configuration B. It should be noted that the passage mean velocity is half that of Configuration A because of the expansion in flow area. Figure 9 shows the mean and rms velocity contours obtained at location B1, 1 D downstream of the inlet. In contrast to Configuration A, the streamwise velocity contours show that the high velocity region is close to the lower wall. This is consistent with the flow characteristics exiting an S-bend. Comparison of the streamwise velocity of Figures 9 and 4 shows that there is a greater vertical velocity variation at the inlet for Configuration B. The maximum streamwise velocity achieves  $0.65 U_b$  (30 % higher than the local mean velocity for Configuration B, in contrast to the 10 % observed in Configuration A). The vertical velocity contours indicate that the S-bend directs the center flow downward and the near-wall flow upward. The maximum positive and negative velocities reach values of  $\pm 0.15 U_b$ , corresponding to 30 % of the local velocity. The increase in streamwise flow non-uniformity and vertical

velocity at the inlet is attributed to a 50% reduction in the inflow bulk mean because of the expansion in flow area between Configurations A and B. The Configuration B flow is more sensitive to secondary flow as a result of the reduction in flow momentum.

Figure 10 shows the mean and rms velocity contours obtained at location B2, 7 D downstream of the inlet. Comparison of the streamwise velocity contours at 1 and 7 diameter downstream of the inlet show convection from upper to lower wall. The high velocity region remains close to the lower wall and the maximum velocity has increased from  $0.65 U_b$  to  $0.80 U_b$  within 6 D. This is attributed to vertical convection. The vertical velocity contour shows upward velocity reaching  $0.95 U_b$  near the two side walls and downward velocity of around  $0.6 U_b$  in the center of the passage, indicating the presence of a double vortex. Comparison of the vertical velocity contours of Figures 10 and 5 shows that the strength of the vortex in the middle of the first passage for the  $1.0'' \times 0.5''$  and  $0.5'' \times 0.5''$  passages is almost equal. However, the double vortex in Configuration B circulates in the opposite direction of Configuration A because the trips skew in the opposite direction. This result indicates that the secondary flow generated by the trips is dependent on trip orientation.

Figure 11 shows the mean and rms velocity contours obtained at location B3, 1 D upstream of the first turn. Comparison of the streamwise velocity contours of Figures 10 and 11 shows reduced streamwise flow development in the next 4 D of the passage. The maximum velocity remains at  $0.8 U_b$  and close to the lower wall. Comparison of the vertical velocity contours of Figures 10 and 11 indicates a substantial reduction in the strength of the double vortex.

Figure 12 shows the mean and rms velocity contours obtained at location B5, 1 D downstream of the first turn. As in Configuration A, the bend radically changes the flow. The streamwise velocity contours at this location (and those of Figure 13) are negative because the second passage is a radially inward flow passage. Comparison of the streamwise velocity contours of Figures 11 and 12 shows that a high velocity region enters and exits the first turn on the concave side, the pressure surface. The high velocity region increases in size and the absolute value has increased from  $0.8 U_b$  to  $1.0 U_b$ : indicating, as expected, further convection from suction to pressure side of the turn. The streamwise velocity contours of Figure 12 also show recirculation of the order of  $0.25 U_b$  (50 % of the passage mean velocity) near the lower wall. The sharp turning of the cross-flow induces separation and the separation bubble occupies up to 30 % of the passage height. The vertical velocity contours show maximum upward velocity of the order of  $0.25 U_b$  in the center of the passage and maximum downward velocity of the order of  $0.6 U_b$  near the two side walls. The circulation direction of the double vortex is opposite to that in the first passage. The secondary flow generated by the trips is also dependent on flow direction.

Figure 13 shows the mean and rms velocity contours obtained at location B6, 1 D upstream of the second turn. Comparison of the streamwise velocity contours of Figures 12 and 13 shows redistribution of the high velocity to the lower wall. This is consistent with the circulation direction of the double vortex. Comparison of Figs. 11 and 13 shows the same pattern inverted. This inversion is due to the change in the trip orientation from the first to the second legs, as opposed to Configuration A (see Figs. 1 and 2 for trip direction). Comparison of the vertical velocity contours of Figures 12 and 13 with Figure 10 shows the vortex strength in the second passage is considerably weaker than that in the first. This phenomenon may be due to the effect of the turns.

Figure 14 shows the mean and rms velocity contours obtained at location B8, 1 D downstream of the third turn. Comparison of the streamwise velocity contours of Figures 13 and 14 shows that the high velocity region enters the second turn on the convex side, the suction side, and exits it on the concave side, the pressure side. As expected, the high velocity region is on the upper wall, concave side of the turn. The maximum absolute streamwise velocity region increases from  $1.00 U_b$  to  $1.65 U_b$  as a result of further convection from suction to pressure side and reduction of flow area. Separation does not occur at the second turn because of the contraction. The vertical velocity contours show negative velocity achieving  $-0.80 U_b$  close to the side walls and positive velocity achieving  $0.60 U_b$  in the center. As expected, the circulation direction of the double vortex is the same as that in the second passage (both trip orientation and flow direction are reversed) but opposite to that of the first (only trip orientation is reversed).

Heat transfer in stationary experiments with augmentation devices on the passage walls is primarily a function of the Reynolds number (a flow parameter), the streamwise velocity distance from the inlet,  $x/D$  (a geometric parameter), and the geometry of the augmentation devices, Johnson, et al (1994). The heat transfer results of Johnson, et al (1994) were obtained within a  $0.5'' \times 0.5''$  square passage at a Reynolds number of 25,000. The trip streamwise pitch to trip height ( $P/e$ ) was 10 and trip height to coolant passage width ( $e/Z$ ) was 0.1. The velocity measurements of Configuration A were obtained with the same Reynolds number, passage cross-sectional area and trip orientation. In the present experiment, the trip streamwise pitch to trip height ( $P/e$ ) was 5 and trip height to coolant passage width ( $e/Z$ ) was 0.1.

The heat transfer results of Johnson, et al (1994) show that, with skewed trip strips, the heat transfer from the leading and trailing walls in the first two legs is three times higher than that with the smooth wall. The increase in surface area (5 % according to Johnson, et al (1994)) associated with the trips and increase in flow velocity (20 % - i.e 16 % increase in heat transfer) due to the blockage of the trip are expected to contribute to the increase in heat transfer. These increases cannot account for the 300 % increase observed in the results of Johnson, et al (1994).

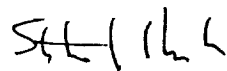
It is evident from the results of Figures 4 to 8 that very strong secondary flow is being generated by the trips, even in the absence of rotation. The trips generate a double vortex of which circulation direction is dependent on flow direction and trip orientation. In the Configuration A measurements, the flow direction and trip orientation give rise to a double vortex with upward velocity of  $0.60 U_b$  in the center and downward velocity of  $-0.95 U_b$  near the leading and trailing walls, explaining the augmented heat transfer data of Johnson, et al (1994). The compressible flow simulation in Tse, et al (1994) shows that near-wall secondary flow of the order of 30 % can lead to a 24 % increase in heat transfer. The effect of near-wall secondary flow of the order of  $0.95 U_b$  on heat transfer can be potentially large. The development of streamwise flow in the first two passages is very significant, as a consequence of the strong secondary flow. The trips generated two high velocity regions (both reaching  $1.50 U_b$ ) close to the leading and trailing walls. The velocity measurements of Tse, et al (1994) show that, for the model with smooth walls, the high velocity region ( $1.25 U_b$ ) is at the center of the passage and the velocity at the boundary layer near the walls is below  $0.8 U_b$ . Based upon the  $Nu-Re^{0.8}$  relationship, the change in flow characteristics led to a 66 % increase in heat transfer. Therefore, most of the increase in heat transfer with skewed trips compared to smooth walls is attributed to change in flow characteristics and the strong secondary flow presence of the double vortex.

Current costs and work accomplished are consistent with those of the original schedule, as shown in Report 533P. Costs to date are slightly greater (by approximately 20%) with work accomplished as per original estimates (see 533P). However, use of a double model will decrease the cost of taking the Task IV rotating measurements. No change is estimated in the original estimate for cost to complete the contract.

The technical effort in the next reporting period will focus on Task 4 (Rotating Measurements).

At the end of the reporting period, approximately 38% of the contract effort has been completed.

Very truly yours,



Stephen J. Shamroth,  
President

SJS:jc

R94-9089-6  
December 13, 1994  
Page 7

cc: Procurement Assistant, M.S. 500-305 (2 copies)

NASA Ctr. For AeroSpace Info. (CASI) (2 copies)  
Attn: Accessioning Dept.  
800 Elkridge Landing Rd.  
Linthicum Heights, MD 21090-2934

Gary Steuber - P&W  
Diane McGrath - P&W  
Joel Wagner - UTRC



**TABLE 1**

<b>Location</b>	
<b>A1, B1</b>	<b>1 D downstream of inlet</b>
<b>A2, B2</b>	<b>7 D downstream of inlet</b>
<b>A3, B3</b>	<b>1 D upstream of the first turn</b>
<b>A4, B4</b>	<b>First turn</b>
<b>A5, B5</b>	<b>1 D downstream of the first turn</b>
<b>A6, B6</b>	<b>1 D upstream of the second turn</b>
<b>A7, B7</b>	<b>Second turn</b>
<b>A8, B8</b>	<b>1 D downstream of the second turn</b>
<b>A9, B9</b>	<b>1 D upstream of the third turn</b>
<b>A10, B10</b>	<b>Third turn</b>
<b>A11, B11</b>	<b>1 D downstream of the third turn</b>
<b>A12, B12</b>	<b>1 D upstream of exit</b>

**Measurement will be obtained without a inlet screen**

**Repeat A1 to A3 and B1 and B3 with an inlet screen**

## List Of Figures

- 1 Measuring location for Case A
- 2 Measuring location for Case B
- 3 Coordinate system
- 4 Velocity contours at A1
- 5 Velocity contours at A2
- 6 Velocity contours at A3
- 7 Velocity contours at A5
- 8 Velocity contours at A6
- 9 Velocity contours at B1
- 10 Velocity contours at B2
- 11 Velocity contours at B3
- 12 Velocity contours at B5
- 13 Velocity contours at B6
- 14 Velocity contours at B8

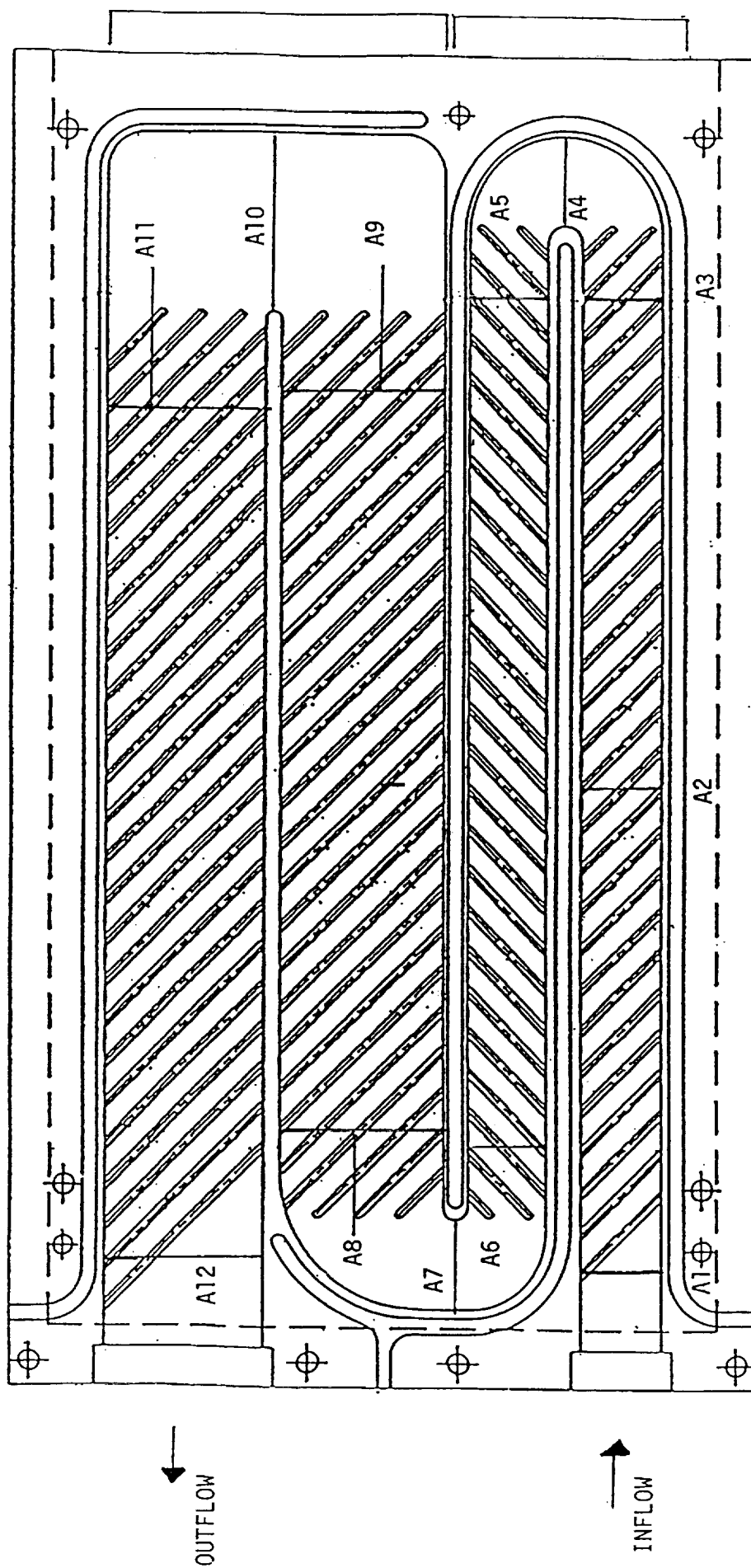


FIGURE 1 - Measuring location for Case A

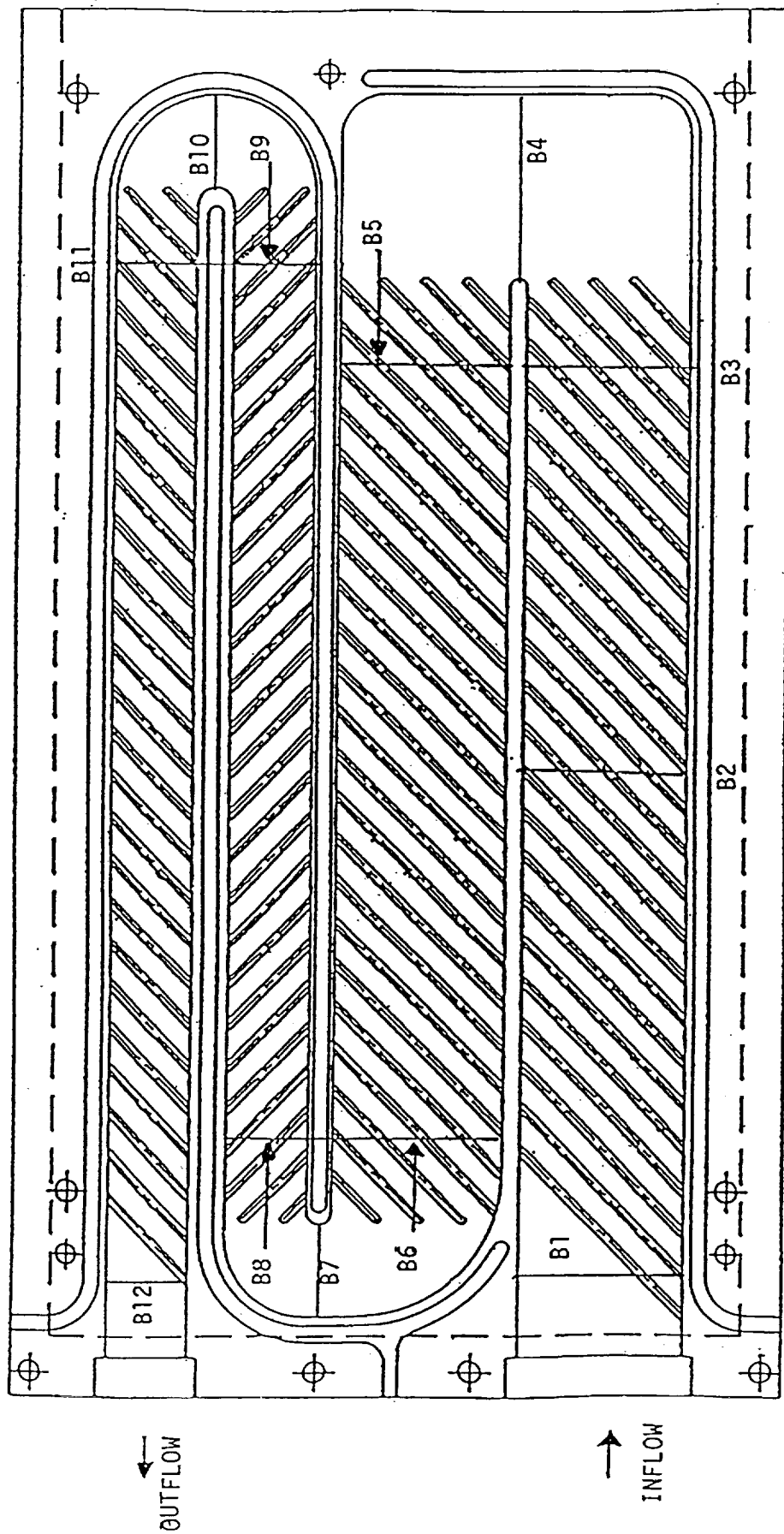


FIGURE 2 - Measuring location for Case B

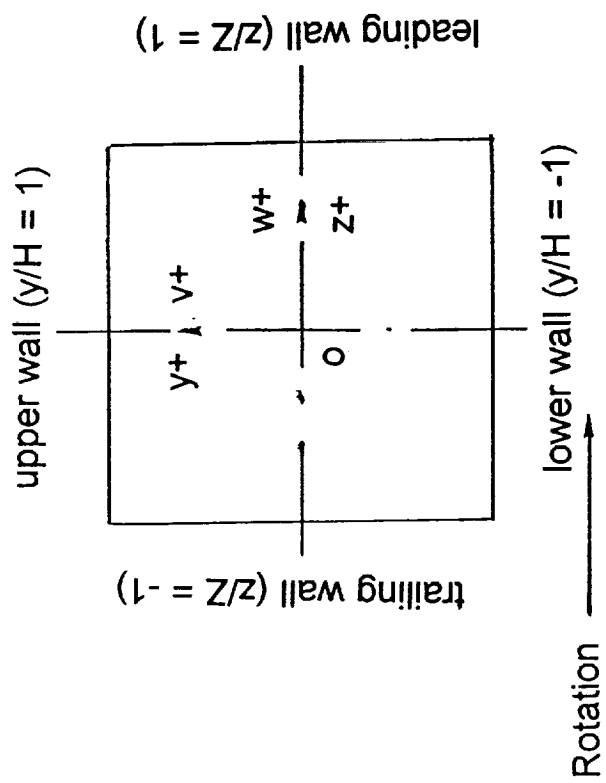
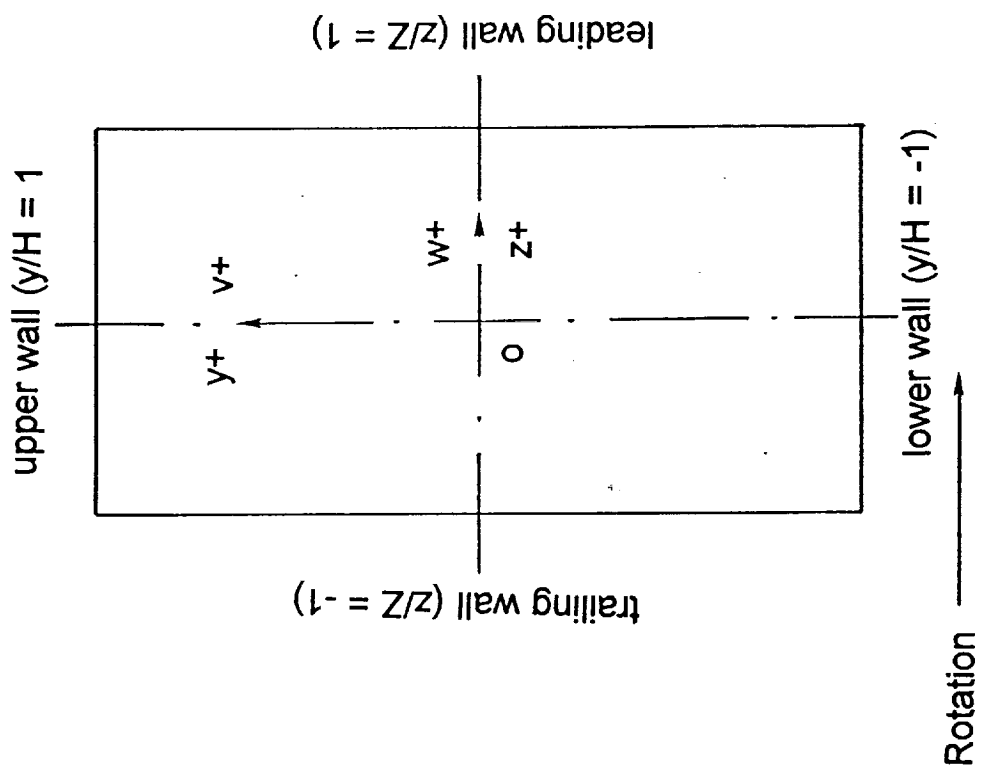
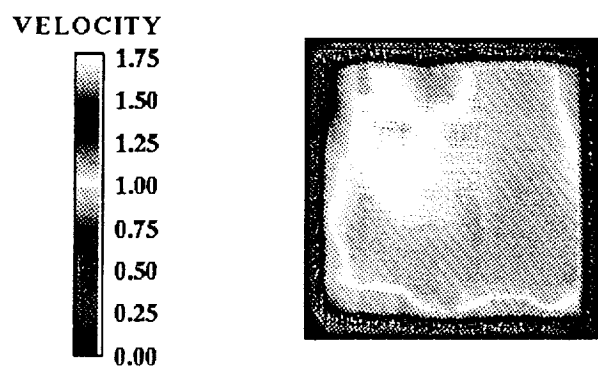
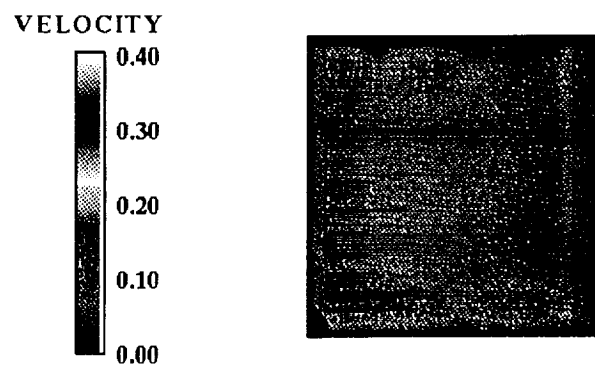


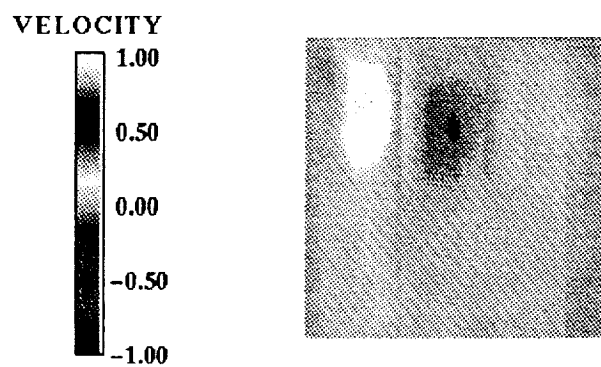
FIGURE 3



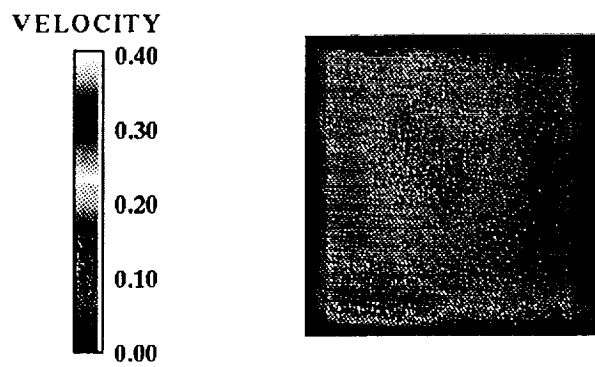
Streamwise Mean Velocity



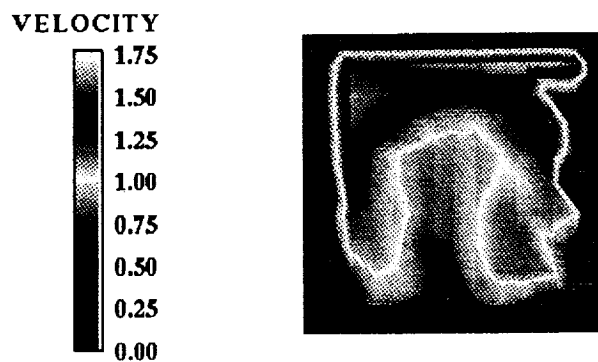
Streamwise RMS Velocity



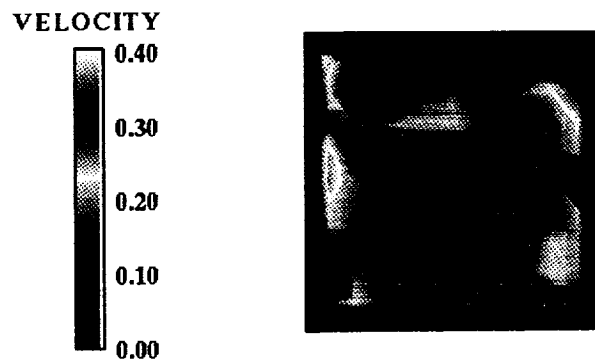
Vertical Mean Velocity



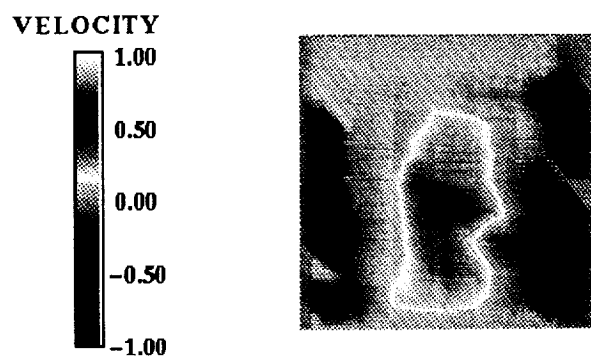
Vertical RMS Velocity



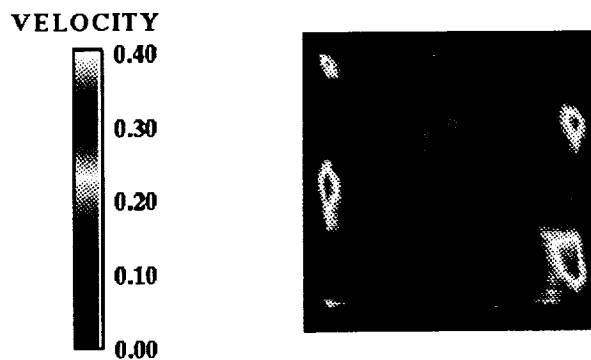
Streamwise Mean Velocity



Streamwise RMS Velocity

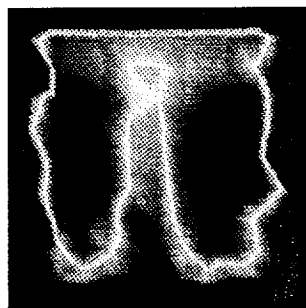
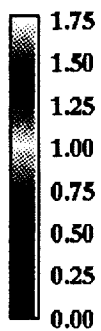


Vertical Mean Velocity



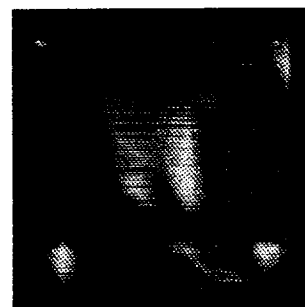
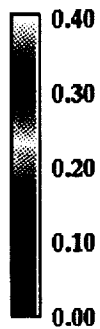
Vertical RMS Velocity

VELOCITY



**Streamwise Mean Velocity**

VELOCITY



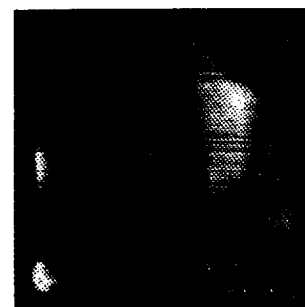
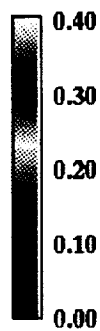
**Streamwise RMS Velocity**

VELOCITY



**Vertical Mean Velocity**

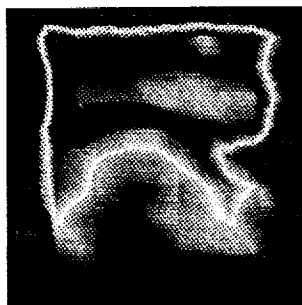
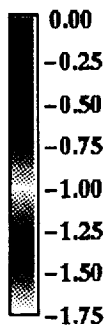
VELOCITY



**Vertical RMS Velocity**

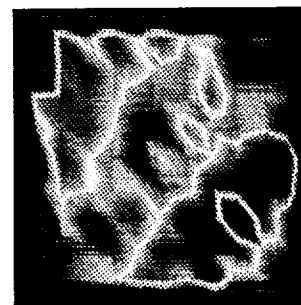
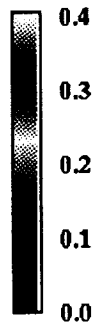


VELOCITY



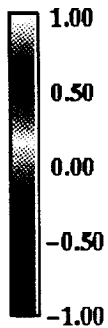
Streamwise Mean Velocity

VELOCITY



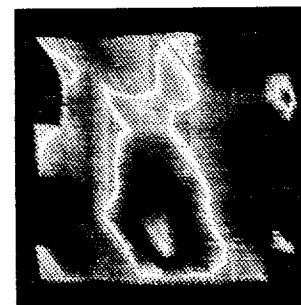
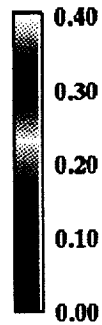
Streamwise RMS Velocity

VELOCITY



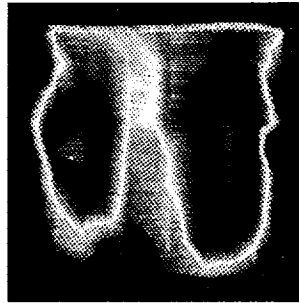
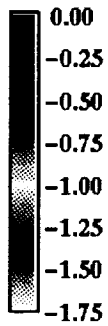
Vertical Mean Velocity

VELOCITY



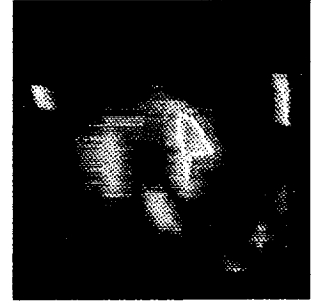
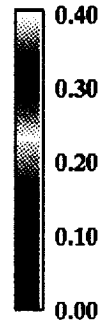
Vertical RMS Velocity

VELOCITY



Streamwise Mean Velocity

VELOCITY



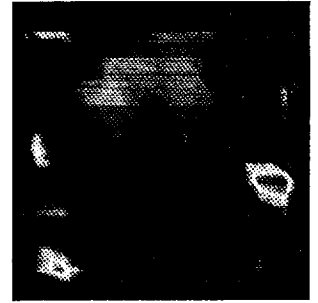
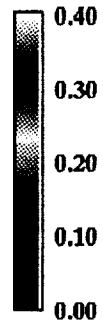
Streamwise RMS Velocity

VELOCITY



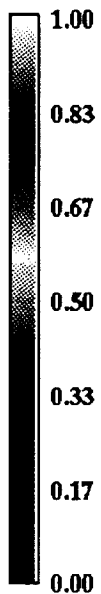
Vertical Mean Velocity

VELOCITY



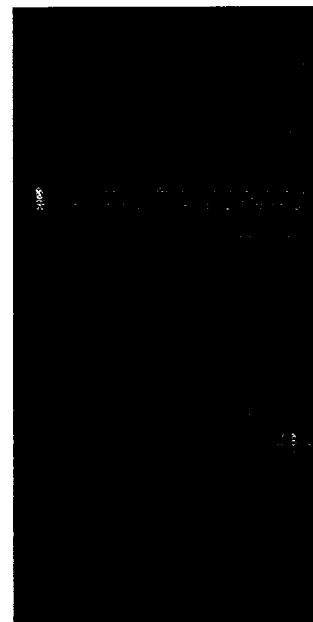
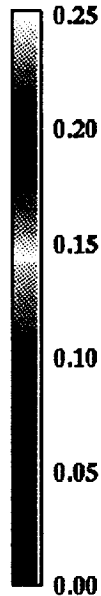
Vertical RMS Velocity

VELOCITY



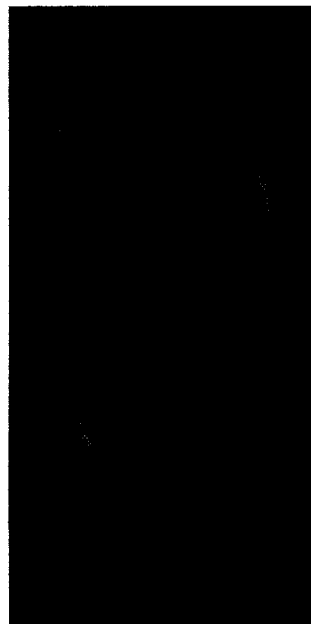
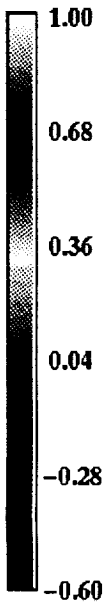
**Streamwise Mean Velocity**

VELOCITY



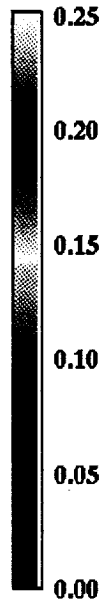
**Streamwise RMS Velocity**

VELOCITY

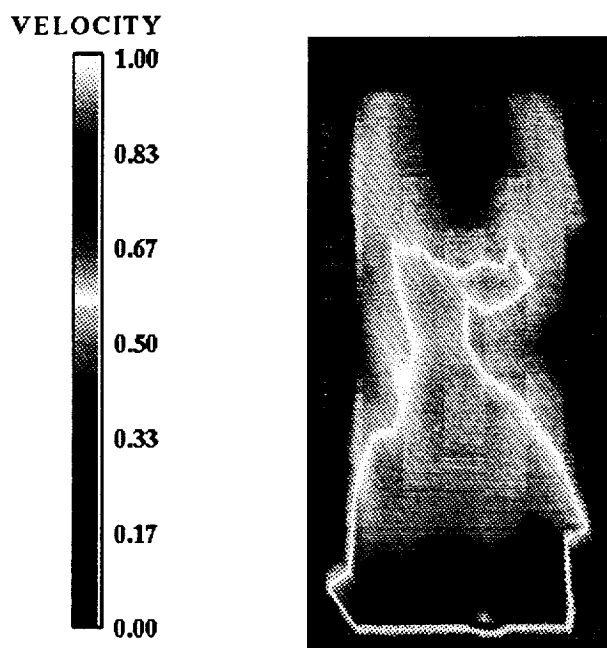


**Vertical Mean Velocity**

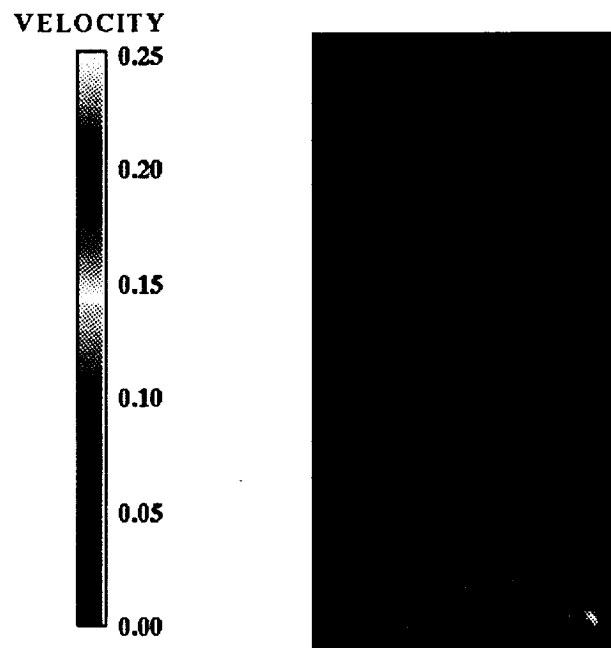
VELOCITY



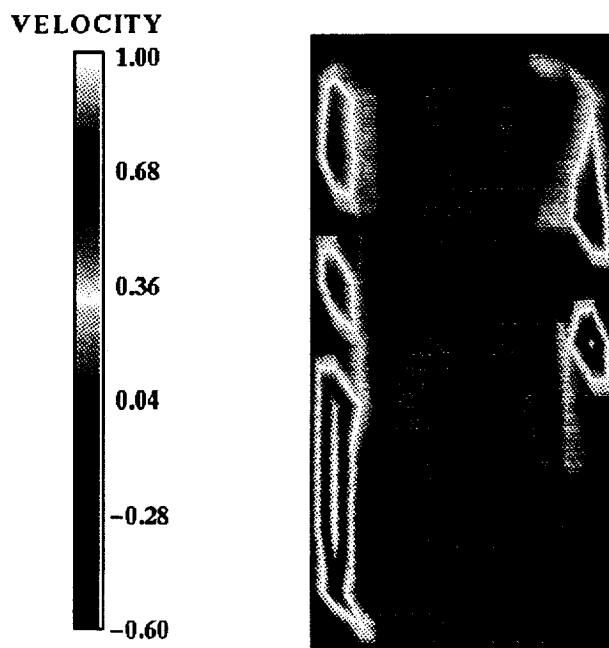
**Vertical RMS Velocity**



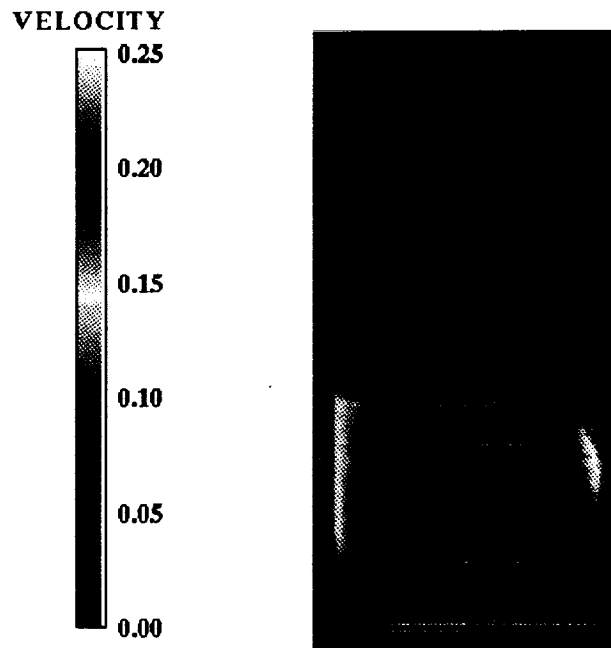
**Streamwise Mean Velocity**



**Streamwise RMS Velocity**

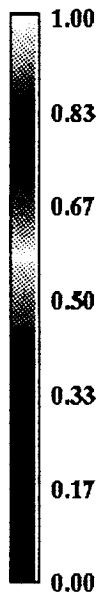


**Vertical Mean Velocity**



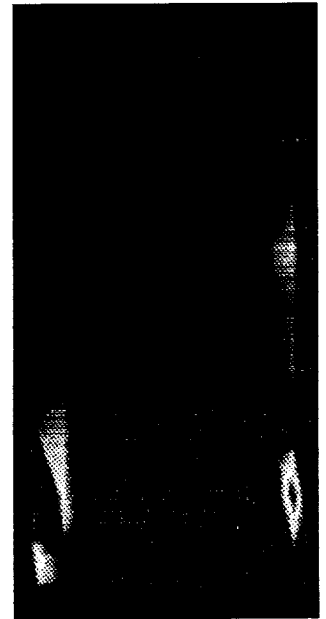
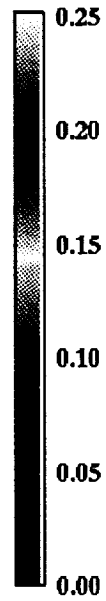
**Vertical RMS Velocity**

VELOCITY



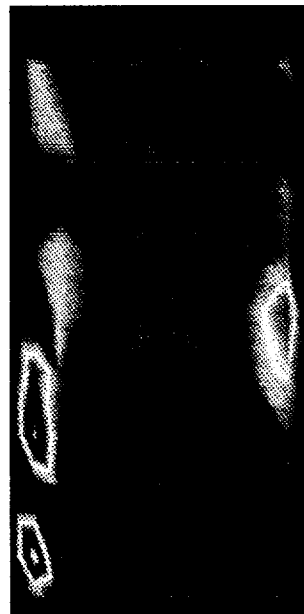
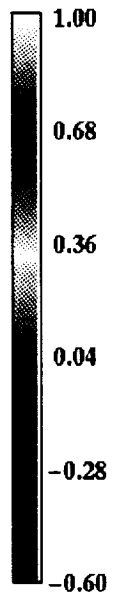
Streamwise Mean Velocity

VELOCITY



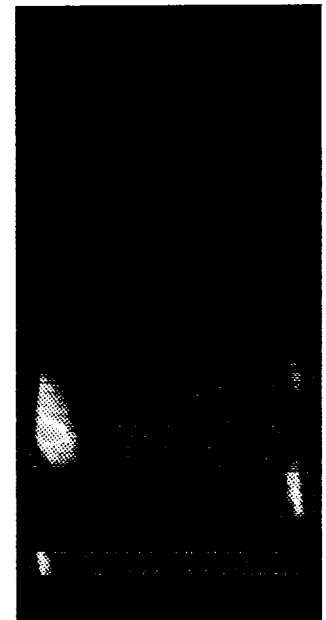
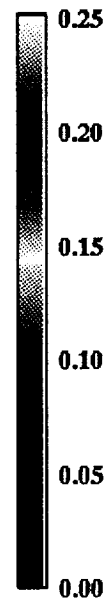
Streamwise RMS Velocity

VELOCITY



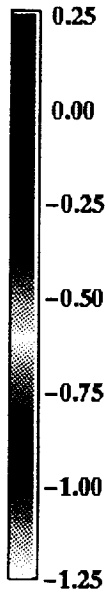
Vertical Mean Velocity

VELOCITY



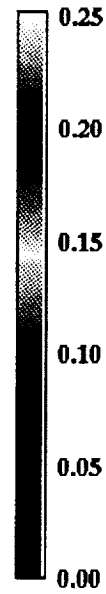
Vertical RMS Velocity

VELOCITY



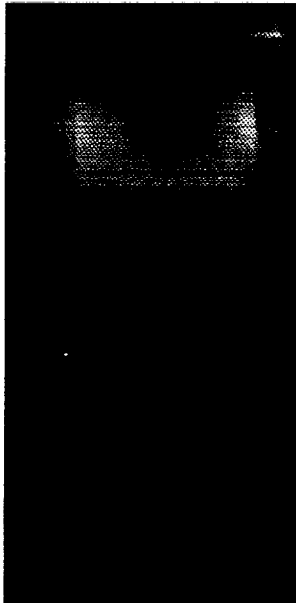
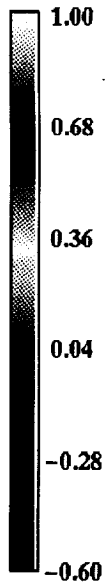
Streamwise Mean Velocity

VELOCITY



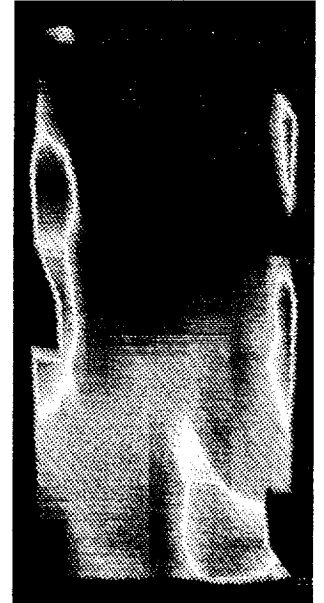
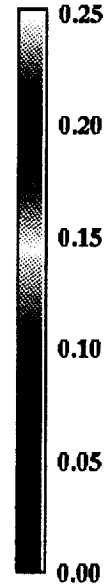
Streamwise RMS Velocity

VELOCITY



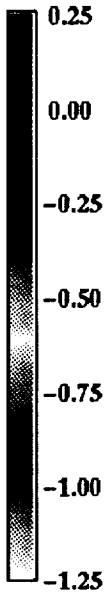
Vertical Mean Velocity

VELOCITY



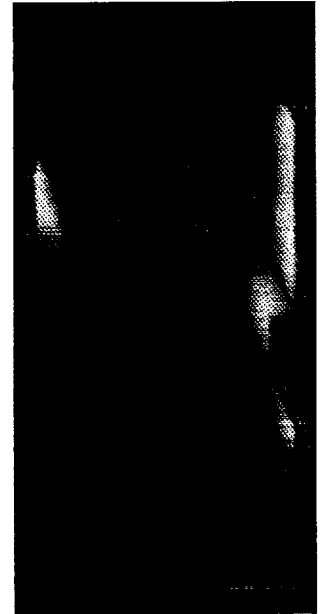
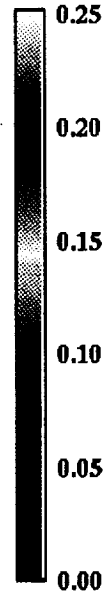
Vertical RMS Velocity

VELOCITY



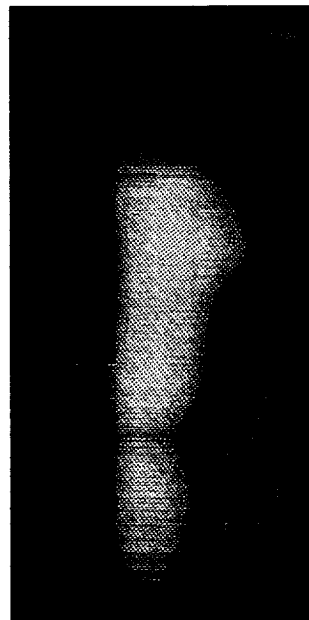
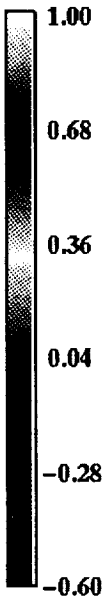
**Streamwise Mean Velocity**

VELOCITY



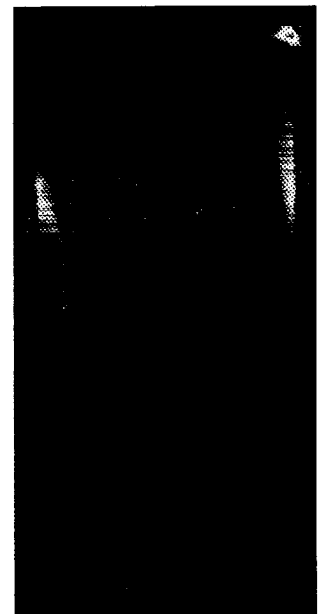
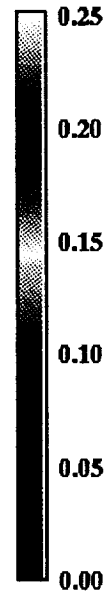
**Streamwise RMS Velocity**

VELOCITY



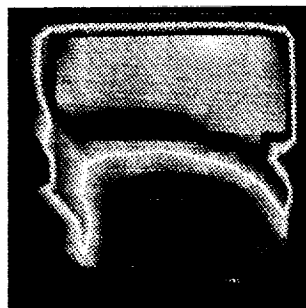
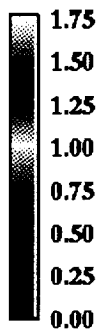
**Vertical Mean Velocity**

VELOCITY



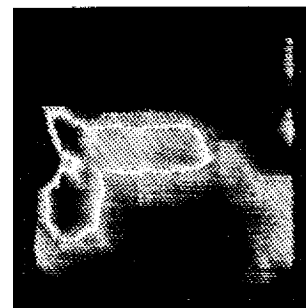
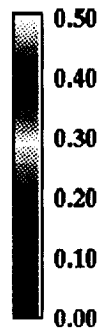
**Vertical RMS Velocity**

VELOCITY



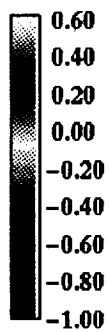
Streamwise Mean Velocity

VELOCITY



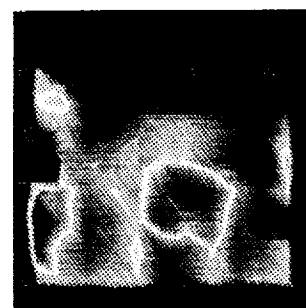
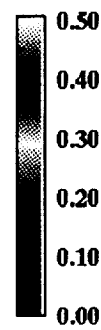
Streamwise RMS Velocity

VELOCITY



Vertical Mean Velocity

VELOCITY



Vertical RMS Velocity